Food Bioprocess Technol (2011) 4:544–558
DOI 10.1007/s11947-009-0187-x

ORIGINAL PAPER

Experimental and Numerical Analysis of Microwave Heating of Water and Oil Using a Rectangular Wave Guide: Influence of Sample Sizes, Positions, and Microwave Power

W. Cha-um · P. Rattanadecho · W. Pakdee

Received: 20 August 2008 / Accepted: 20 January 2009 / Published online: 13 March 2009

Abstract The heating process of water and oil using microwave oven with rectangular wave guide is investigated numerically and experimentally. The numerical model is validated with an experimental study. The transient Maxwell's equations are solved by using the finite difference time domain method to describe the electromagnetic field in the wave guide and sample. The temperature profiles and velocity field within sample are determined by the solution of the momentum, energy, and Maxwell's equations. In this study, the effects of physical parameters, e.g., microwave power, the position of sample in wave guide, size, and thickness of sample, are studied. The results of distribution of electric field, temperature profiles, and velocity field are presented in details. The results show that the mathematical models are in agreement with the experimental data. Conclusively, the mathematical model presented in this study correctly explains the phenomena of microwave heating within the liquid layer.

Keywords Microwave heating · Rectangular wave guide · Mode TE_{10} · Maxwell's equation · FDTD method

Nomenclature

C_p	specific heat capacity [J/(kg K)]
E	electric field intensity (V/m)
f	frequency of incident wave (Hz)
g	gravitational constant (m/s^2)
H	magnetic field intensity (A/m)
P	power (W)
p	pressure (Pa)
Q	local electromagnetic heat generation term (W/m^3)
s	Poynting vector (W/m^2)
T	temperature (°C)
t	time (s)
tan δ	dielectric loss coefficient (−)
u,w	velocity component (m/s)
Z_H	wave impedance (Ω)
Z_I	intrinsic impedance (Ω)

Greek letters

α	thermal diffusivity (m^2/s)
β	coefficient of thermal expansion (1/K)
η	absolute viscosity (Pa s)
ε	permittivity (F/m)
λ	wavelength (m)
μ	magnetic permeability (H/m)
υ	velocity of propagation (m/s)
ν	kinematics viscosity (m^2/s)
ρ	density (kg/m^3)
σ	electric conductivity (S/m)
ω	angular frequency (rad/s)
ξ	surface tension (N/m)

Subscripts

∞	ambient condition
a	air
j	layer number
in	input
w	water

W. Cha-um · P. Rattanadecho (✉) · W. Pakdee
Research Center of Microwave Utilization in Engineering (RCME), Department of Mechanical Engineering,
Faculty of Engineering, Thammasat University (Rangsit Campus),
Pathumthani 12120, Thailand
e-mail: ratphadu@engr.tu.ac.th

Introduction

Microwave is a one heat source that is an attractive alternative over conventional heating methods because an

electromagnetic wave that penetrates the surface is converted into thermal energy within the material. High speed startup, selective energy absorption, instantaneous electric control, non-pollution, high energy efficiency, and high product quality are several advantages of microwave heating. Therefore, this technology is used in many industrial and household applications. The notable application is the domestic microwave oven. In addition, it has been used in food industry for drying, pasteurization, sterilization, etc. (Chatterjee et al. 2007). Other uses include vulcanization processing, curing of concrete, medical sterilization, and process adhesives.

Referred to international journals in the past about microwave heating process, the microwave power absorbed was assumed to decay exponentially into the sample following the Lambert's law. For example, Datta et al. (1992) predicted the volumetric heat source by using Lambert's law and analyzed the temperature profiles in liquid. However, this assumption is valid for the large dimension samples where the depth of sample is much larger than the penetration depth, but for the thin samples, where the depth of sample is much smaller than penetration depth, heat transfer rate by microwave is faster. Therefore, the spatial variations of the electromagnetic field within thin samples must be obtained by solution of the Maxwell's equations. The models of the interactions between electromagnetic field and dielectric materials have been used previously to study numerous heating processes of dielectric materials in a variety of microwave applicator, such as rectangular wave guide and cavities. Jia et al. (1992), Liu et al. (1994), and Dibben and Metaxas (1997) showed the numerical modeling of microwave heating process in cavity by solving Maxwell's equation, which determines the electromagnetic field in the microwave applicator and wave guide. Ayappa et al. (1994) studied the two-dimensional natural convection of liquid in a square cavity that exposed to traveling plane microwave numerically. They found that the location, intensity, and number of power peaks influence a uniformity of temperature in liquid. Basak and Ayappa (2002) purposed the modeling to study the role of length scales on microwave thawing process in 2D cylinders. From their investigation, thawing time increased monotonically with sample diameter, and temperature gradients in the sample generally increased from regimes I to III. Tada et al. (1997) used 2D finite difference time domain (2D-FDTD) method to investigate the electromagnetic field in microwave applicator filled partially with a dielectric material. This work demonstrated the effects of the position of dielectrics on energy absorption ratio. Zhang et al. (2000) purposed 3D-FDTD to explain the distribution of microwave inside the cavity by solving the Maxwell's equation and using the finite control volume (FCV) method based on SIMPLER algorithm to obtain temperature profiles and flow field for distilled water and corn oil. Ratanadecho et al. (2002a,b) numerically and experimentally investigated microwave heating of a liquid layer in a rectangular wave guide. Their work showed both of the electric conductivity and microwave power level that affected the degree of penetration and rate of heat generation within liquid layer. Chatterjee et al. (2007) illustrated effect of turntable rotation, natural convection, power source, and aspect ratio of container on the temperature profiles in heating of containerized liquid using microwave radiation by using numerical simulation. Zhu et al. (2007) presented numerical model of heat transfer in liquids that flow continuously in a circular duct. The results showed that the heating pattern strongly depends on the dielectric properties of the fluid in the duct and the geometry of microwave heating system. Curet et al. (2008) studied a microwave heating process in frozen and defrosted zone considering both a numerical and experimental aspects. Either Maxwell's equation or Lambert's law were used to model the microwave heat generation. Huo et al. (2004) presented a 3D finite element-boundary integral formulation. Computed results were presented for the electric field distribution, power absorption, and temperature distribution in a food load thermally treated in an industrial pilot scale microwave oven designed for food sterilization. Rattanadecho (2006) presented the modeling of microwave heating of wood using a rectangular wave guide. The influence of irradiation times, working frequencies, and sample size were examined. The presented modeling is used to identify the fundamental parameters and provide guidance for microwave heating of wood. Ratanadecho et al. (2002a,b) studied the melting of frozen packed beds by a microwave with a rectangular wave guide numerically and experimentally. They focused on the prediction of temperature, as well as the microwave energy absorbed, and the melting front within the layered packed beds. Based on the combined model of the Maxwell and heat transport equations, the results showed that the direction of melting against the incident microwave strongly depended on the structural-layered packed beds. In addition, there are many papers in this field, such as Basak (2003–2004), Ratanadecho et al. (2002a,b), Rattanadecho and Suwannapum (2009), Vadivambal and Jayas (2009), and Boyacı et al. (2009).

Nevertheless, most of the studies have concentrated on solids and focused on conduction mode heat transfer in a specimen. A few papers have investigated natural convection induced by microwave heating of liquids in a rectangular wave guide with a full comparison between mathematical modeling and experimental data. This is because of the complex distribution of electromagnetic wave in cavity that is a complicated effect on flow field.

However, this paper presents distributions of electric field, temperature profiles, and flow pattern. This work is

extended from the previous work of Ratanadecho et al. (2002a,b). The goal of this work is to analyze microwave heating processes using a mathematical model. The effects of microwave power level (300, 500, 800, and 1,000 W) and the position in wave guide are investigated. The positions of the center of the liquid layer is at the centerline of the wave guide (S0) and also at 10 mm (S10) and 20 mm (S20) away from the centerline. Moreover, effects of liquid layer size (half and equal to wave guide width) and thickness (30, 40, and 50 mm) are studied.

Experiment Setup

The experimental apparatus is shown in Fig. 1. The microwave system is a monochromatic wave of TE_{10} mode operating at a frequency of 2.45 GHz. Magnetron generates microwave and transmits along the z-direction of the rectangular wave guide, with inside dimensions of 109.2 (X) mm × 54.61(Y) mm^2 toward a water load that is situated at the end of the wave guide. On the upstream side of the sample, an isolator is used to trap any microwave reflected from the sample to prevent the microwave from damaging the magnetron. The powers of incident and the reflected and transmitted waves are measured by a wattmeter using a directional coupler (Micro Denshi., model DR-5000). Fiberoptic (Luxtron Fluroptic Thermometer., model 790, accurate to ±0.5°C) is employed for temperature measurement. The fiberoptic probes are inserted into the sample and situated on the XZ plane at Y=25 mm. Due to the symmetrical condition, temperatures are measured for only one side of the plane. An initial temperature of sample is 28°C for all cases. A sample container with a thickness of 0.75 mm is made from polypropylene, which does not absorb microwaves.

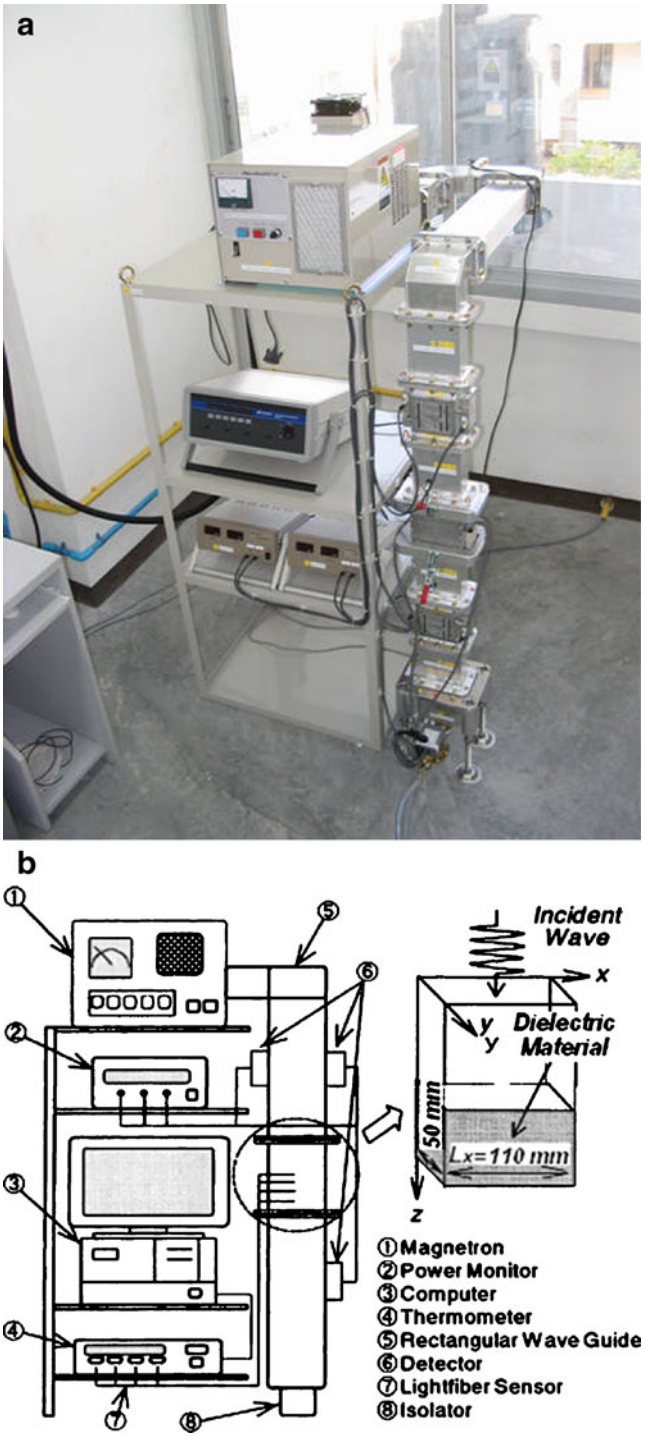

Fig. 1 Experimental apparatus of microwave heating: **a** picture, **b** diagram

Mathematical Model Formulation

Figure 2a and b shows the schematic diagram of the problem in case of full and partial load, respectively. The case of full load is the condition in which the liquid layer cross-sectional area is 109.2(X)×54.61(Y) mm^2 the same as that of the wave guide, while partial load corresponds to liquid layer with a half cross-sectional area of 54.61(X)× 54.61(Y) mm^2. Inside the wave guide, the sample is contained in a container, whose walls are insulated except the top wall.

Analysis of Electromagnetic Field

Since the electromagnetic field that is investigated is the microwave field in the TE_{10} mode, there is no variation of field in the direction between the broad faces of the rectangular wave guide and is uniform in the y-direction. Consequently, it is assumed that the 2D heat transfer model in x and z-directions would be sufficient to identify the microwave heating phenomena in a rectangular wave guide

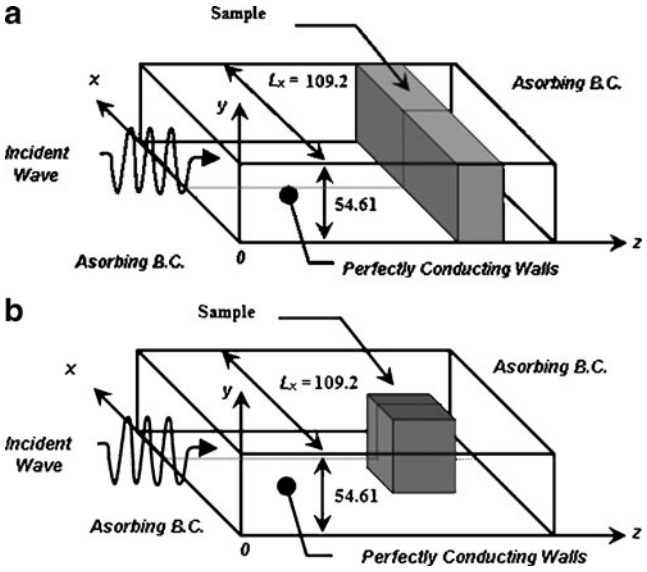

Fig. 2 Schematic diagram of the problem: **a** full load case, **b** partial load case

(Rattanadecho et al. 2002). The other assumptions are as follows:

1. The absorption of microwave by air in a rectangular wave guide is negligible.
2. The walls of rectangular wave guide are perfect conductors.
3. The effect of sample container on the electromagnetic and temperature field can be neglected.

The proposed model is considered in TE_{10} mode so that the Maxwell's equations can be written in terms of the electric and magnetic intensities

$$\varepsilon\frac{\partial E_y}{\partial t}=\frac{\partial H_x}{\partial z}-\frac{\partial H_z}{\partial x}-\sigma E_y \tag{1}$$

$$\mu\frac{\partial H_z}{\partial t}=-\frac{\partial E_y}{\partial x} \tag{2}$$

$$\mu\frac{\partial H_x}{\partial t}=\frac{\partial E_y}{\partial z} \tag{3}$$

where E and H denote electric and magnetic field intensities, respectively. Subscripts x, y, and z represent x, y, and z components of vectors, respectively. Furthermore, ε is the electrical permittivity, σ is the electrical conductivity, and μ is the magnetic permeability. These symbols are

$$\varepsilon=\varepsilon_0\varepsilon_r \tag{4}$$

$$\mu=\mu_0\mu_r \tag{5}$$

$$\sigma=2\pi f\varepsilon\tan\delta \tag{6}$$

When the material is heated unilaterally, it is found that as the dielectric constant and loss tangent coefficient vary, the penetration depth and the electric field within the dielectric material vary. The penetration depth is used to denote the depth at which the power density has decreased to 37% of its initial value at the surface (Ratanadecho et al. 2002a,b).

$$D_p=\frac{1}{\frac{2\pi f}{\upsilon}\sqrt{\frac{\varepsilon_r'\left(\sqrt{1+\left(\frac{\varepsilon_r''}{\varepsilon_r'}\right)^2}-1\right)}{2}}}=\frac{1}{\frac{2\pi f}{\upsilon}\sqrt{\frac{\varepsilon_r'\left(\sqrt{1+(\tan\delta)^2}-1\right)}{2}}} \tag{7}$$

where D_p is penetration depth, ε''_r is relative dielectric loss factor and υ is the microwave speed. The penetration depth of the microwave power is calculated according to Eq. 7, which shows how it depends on the dielectric properties of the material. It is noted that products with huge dimensions and high loss factors may occasionally overheat a considerably thick layer on the outer layer. To prevent such phenomenon, the power density must be chosen so that enough time is provided for the essential heat transfer between boundary and core. If the thickness of the material is less than the penetration depth, only a fraction of the supplied energy will become absorbed. In example, consider that the dielectric properties of water typically show moderate lousiness depending on the temperature. The water layer at low temperature typically shows slightly greater potential for absorbing microwaves. In other words, an increase in the temperature typically decreases ε''_r, accompanied by a slight increase in D_p.

The boundary conditions for TE_{10} mode can be formulated as follows:

1. Perfectly conducting boundary. Boundary conditions on the inner wall surface of wave guide are given by Faraday's law and Gauss's theorem:

$$E_{\parallel}=0, H_{\perp}=0 \tag{8}$$

where subscripts $\parallel$ and $\perp$ denote the components of tangential and normal directions, respectively.

2. Continuity boundary condition. Boundary conditions along the interface between sample and air are given by Ampere's law and Gauss's theorem:

$$E_{\parallel}=E'_{\parallel}, H_{\parallel}=H'_{\parallel} \tag{9}$$

3. Absorbing boundary condition. At both ends of rectangular wave guide, the first order absorbing conditions are applied:

$$\frac{\partial E_y}{\partial t}=\pm\upsilon\frac{\partial E_y}{\partial z} \tag{10}$$

where ± is represented forward and backward direction and υ is velocity of wave.

4. Oscillation of the electric and magnetic intensities by magnetron. For incident wave due to magnetron is given by Ratanadecho et al. (2002a,b)

$$E_y = E_{yin} \sin\left(\frac{\pi x}{L_x}\right) \sin(2\pi f t) \tag{11}$$

$$H_x = \frac{E_{yin}}{Z_H} \sin\left(\frac{\pi x}{L_x}\right) \sin(2\pi f t) \tag{12}$$

where E_{yin} is the input value of electric field intensity, L_x is the length of the rectangular wave guide in the x-direction, Z_H is the wave impedance defined as

$$Z_H = \frac{\lambda_g Z_l}{\lambda} = \frac{\lambda_g}{\lambda}\sqrt{\frac{\mu}{\varepsilon}} \tag{13}$$

In this equation, Z_l is intrinsic impedance depending on the properties of the material, λ and λ_g are the wave lengths of microwaves in free space and rectangular wave guide, respectively.

The power flux associated with a propagating electromagnetic wave is expressed by the Poynting vector:

$$s = \frac{1}{2}\,\mathrm{Re}\left(E \times H^*\right) \tag{14}$$

The Poynting theorem allows the evaluation of the microwave power input. It is represented as

$$P_{in} = \int_A SdA = \frac{A}{4Z_H} E_{yin}^2 \tag{15}$$

Analysis of Temperature Profiles and Flow Field

The analytical model is shown in Fig. 2. To reduce complexity of the problem, several assumptions have been offered into the flow and energy equations:

1. Corresponding to electromagnetic field, considering flow and temperature field can be assumed to be two-dimensional plane.
2. The effect of the phase change for liquid layer can be neglected.
3. Liquid layer is assumed when the Boussinesq approximation is valid.
4. The surroundings of the liquid layer are insulated except at the upper surface where energy exchanges with the ambient air.

Heat Transfer Equation

The temperature of liquid layer exposed to incident wave is obtained by solving the conventional heat transport equation with the microwave power absorbed included as a local electromagnetic heat generation term:

$$\frac{\partial T}{\partial t} + \frac{\partial (uT)}{\partial x} + \frac{\partial (wT)}{\partial z} = \frac{\partial}{\partial x}\left(\alpha \frac{\partial T}{\partial x}\right) + \frac{\partial}{\partial z}\left(\alpha \frac{\partial T}{\partial z}\right) + Q \tag{16}$$

where Q is the local electromagnetic heat generation term, which is a function of the electric field and defined as

$$Q = 2\pi f \varepsilon_0 \varepsilon'_r \tan\delta \left(E_y\right)^2 \tag{17}$$

Flow Field Equation

The governing equations for a Newtonian Boussinesq fluid are given as

Continuity equation:

$$\frac{\partial u}{\partial x} + \frac{\partial w}{\partial z} = 0 \tag{18}$$

Momentum equations:

$$\frac{\partial u}{\partial t} + u\frac{\partial u}{\partial x} + w\frac{\partial u}{\partial z} = -\frac{1}{\rho}\frac{\partial p}{\partial x} + \frac{\partial}{\partial x}\left(\nu \frac{\partial u}{\partial x}\right) + \frac{\partial}{\partial z}\left(\nu \frac{\partial u}{\partial z}\right) \tag{19}$$

$$\frac{\partial w}{\partial t} + u\frac{\partial w}{\partial x} + w\frac{\partial w}{\partial z} = -\frac{1}{\rho}\frac{\partial p}{\partial z} + \frac{\partial}{\partial x}\left(\nu \frac{\partial w}{\partial x}\right) + \frac{\partial}{\partial z} \times \left(\nu \frac{\partial w}{\partial z}\right) + g\beta(T - T_0) \tag{20}$$

where ν and β are the kinematics viscosity and coefficient of thermal expansion of the water layer, respectively.

Boundary and initial conditions for these equations:

Since the walls of container are rigid, the velocities are zero. At the interface between liquid layer and the walls of container, zero slip boundary conditions are used for the momentum equations.

1. At the upper surface, the velocity in normal direction (w) and shear stress in the horizontal direction are assumed to be zero, where the influence of Marangoni flow (Ratanadecho et al. 2002a,b) can be applied:

$$\eta \frac{\partial u}{\partial z} = -\frac{d\xi}{dT}\frac{\partial T}{\partial x} \tag{21}$$

2. The walls, except top wall, is insulated so no heat and mass exchanges:

$$\frac{\partial T}{\partial x} = \frac{\partial T}{\partial z} = 0 \tag{22}$$

3. Heat is lost from the surface via natural convection and radiation:

$$-\lambda\frac{\partial T}{\partial z}=h_c(T-T_\infty)+\sigma_{\mathrm{rad}}\varepsilon_{\mathrm{rad}}T^4 \tag{23}$$

4. The initial condition of a water layer is defined as:

$$T=T_0 \text{ at } t=0 \tag{24}$$

Numerical Solution

The description of heat transport and flow pattern of liquid layer Eqs. 16, 17, 18, 19, and 20 requires specification of temperature (T), velocity component (u, w), and pressure (p). These equations are coupled to the Maxwell's equations (Eqs. 1, 2, and 3) by Eq. 17. It represents the heating effect of the microwaves in the liquid-container domain.

Electromagnetic Equations and FDTD Discretization

The electromagnetic equations are solved by using FDTD method. With this method, the electric field components (E) are stored halfway between the basic nodes, while magnetic field components (H) are stored at the center. Therefore, they are calculated at alternating half-time steps. E and H field components are discretized by a central difference method (second-order accurate) in both spatial and time domain. For TE mode, the electric and magnetic field components are discretized as

$$E_y^n(i,k)=\frac{1-\frac{\sigma(i,k)\Delta t}{2\varepsilon(i,k)}}{1+\frac{\sigma(i,k)\Delta t}{2\varepsilon(i,k)}}E_y^{n-1}(i,k)+\frac{\Delta t}{\varepsilon(i,k)}\frac{1}{1+\frac{\sigma(i,k)}{2\varepsilon(i,k)}}\cdot\left\{\frac{H_z^{n-1/2}(i+1/2,k)-H_z^{n-1/2}(i-1/2,k)}{\Delta x}+\frac{H_x^{n-1/2}(i,k-1/2)-H_x^{n-1/2}(i,k+1/2)}{\Delta z}\right\} \tag{25}$$

$$H_x^{n+1/2}(i,k+1/2)=H_x^{n-1/2}(i,k+1/2)+\frac{\Delta t}{\mu(i,k+1/2)}\left\{\frac{E_y^n(i,k+1)-E_y^n(i,k)}{\Delta z}\right\} \tag{26}$$

$$H_z^{n+1/2}(i+1/2,k)=H_z^{n-1/2}(i+1/2,k)-\frac{\Delta t}{\mu(i+1/2,k)}\left\{\frac{E_y^n(i+1,k)-E_y^n(i,k)}{\Delta x}\right\} \tag{27}$$

Fluid Flow and Heat Transport Equations and Finite Control Volume Discretization

Equations 16, 17, 18, 19, and 20 are solved numerically by using the finite control volume along with the SIMPLE algorithm developed by Patankar. The reason to use this method is the advantage of flux conservation that avoids generation of parasitic source. The basic strategy of the finite control volume discretization method is to divide the calculated domain into a number of control volumes and then integrate the conservation equations over this control volume over an interval of time [t,t + Δt]. At the boundaries of the calculated domain, the conservation equations are discretized by integrating over half the control volume and taking into account the boundary conditions. At the corners of the calculated domain, a quarter of control volume was used. The fully implicit time discretization finite difference scheme is used to arrive at the solution in time. Additionally, the details about numerical discretization of this method can be found in the recent literature.

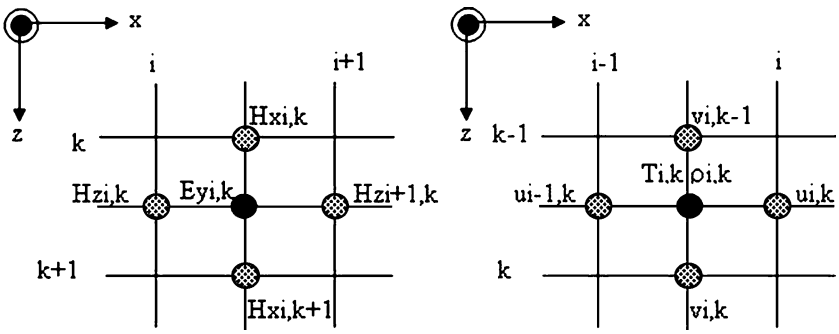

Fig. 3 Grid system configurations

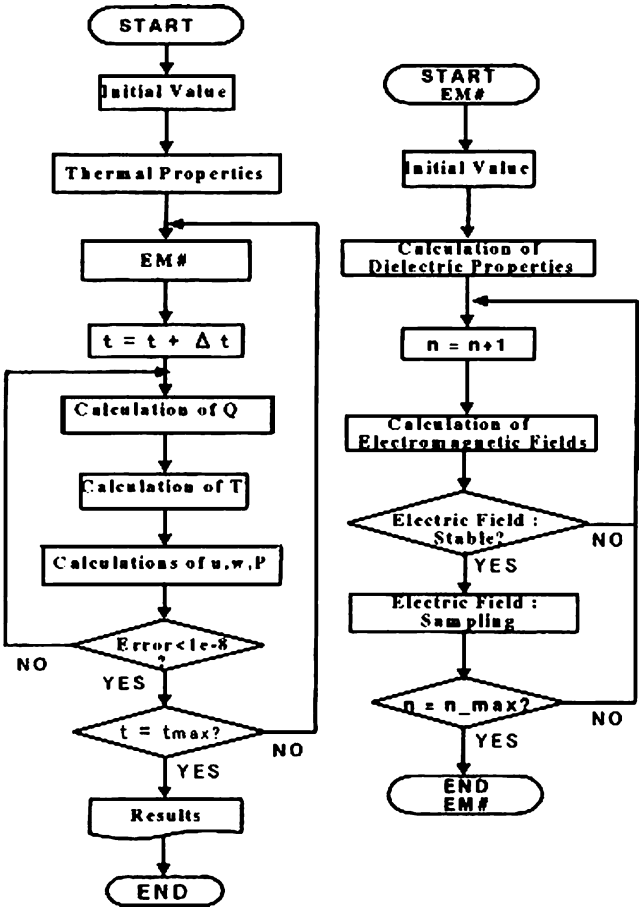

Fig. 4 Computational schemes (*EM#* subroutine for calculation of electromagnetic field; *n* calculation loop of electromagnetic field) (Ratadecho et al. 2002a,b)

The Stability and Accuracy of Calculation

The choice of spatial and temporal resolution is motivated by reasons of stability and accuracy. Spatially, as shown in Fig. 3, Eqs. 25, 26, and 27) are solved on a grid system, and temporally, they are solved alternatively for both the electric and magnetic fields. To ensure stability of the time stepping algorithm Δt must be chosen to satisfy the courant stability condition and defined as

$$\Delta t \leq \frac{\sqrt{(\Delta x)^2+(\Delta z)^2}}{\upsilon} \tag{28}$$

and the spatial resolution of each cell, defined as

$$\Delta x, \Delta z \leq \frac{\lambda_g}{10\sqrt{\varepsilon_r}} \tag{29}$$

Corresponding to Eqs. 28 and 29, the calculation conditions are as follows:

1. Grid size: Δx=1.0922 and Δz=1.0000 mm
2. Time steps: $\Delta t=2\times10^{-12}$ and Δt=0.01 s are used corresponding to electromagnetic field and temperature field calculations, respectively.
3. Relative error in the iteration procedures of 10^{-6} was chosen.

The Iterative Computational Schemes

Since the dielectric properties of liquid layer samples are temperature dependent, to understand the influence of electromagnetic field on microwave heating of liquid layer realistically, it is necessary to consider the coupling between electric field and temperature and fluid flow fields. For this reason, the iterative computational schemes are required to resolve the coupled non-linear Maxwell's equations, momentum, and heat transport equations.

The computational scheme is to first compute a local heat generation term by running an electromagnetic calculation with uniform properties determined from initial temperature data. The electromagnetic calculation is performed until a sufficient period is reached in which representative average root mean square of the electric field at each point is computed and used to solve the time dependent temperature and velocities field. Using these temperatures, new values of the dielectric properties are calculated and used to re-calculate the electromagnetic fields and then the microwave power absorption. All the steps are repeated until the required heating time is reached. The detail of computational schemes and strategy are illustrated in Fig. 4.

Results and Discussion

Two kinds of liquid are simulated in order to display physical phenomena of microwave heating in the liquid

Table 1 The electromagnetic and thermo physical properties used in the computations (Ratanadecho et al. 2002a,b and Aparna et al. 2007)

Property	Air	Water	Oil
Heat capacity, C_p (J kg^{-1} K^{-1})	1,007	4,190	2,000
Thermal conductivity, λ (W m^{-1} K^{-1})	0.0262	0.609	0.168
Density, ρ (kg m^{-3})	1.205	1000	900
Dielectric constant, ε'_r	1.0	$88.15-0.414\ T+(0.131\times10^{-2})T^2-(0.046\times10^{-4})T^3$	2.8
Loss tangent, tan δ	0.0	$0.323-(9.499\times10^{-3})T+(1.27\times10^{-4})T^2-(6.13\times10^{-7})T^3$	0.05

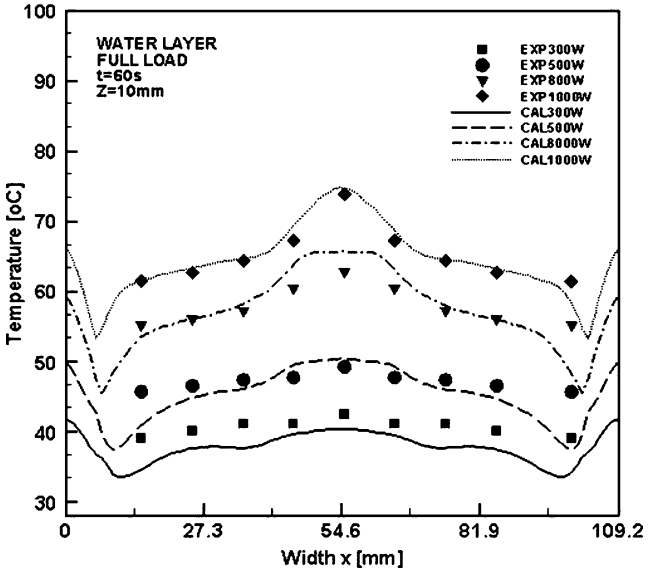

Fig. 5 comparison of the temperature distribution within the water layer between the predicted and experimental results at various microwave power, at t=60 s, along with the horizontal axis (z= 10 mm) of a rectangular wave guide

layers with different dielectric properties. Water and oil are chosen for this purpose. Dimensions of the rectangular wave guide are 109.2(X)×54.61(Y) mm^2. Microwave frequency is operated at 2.45 GHz. Thermal and dielectric properties used for mathematical calculations are shown in Table 1.

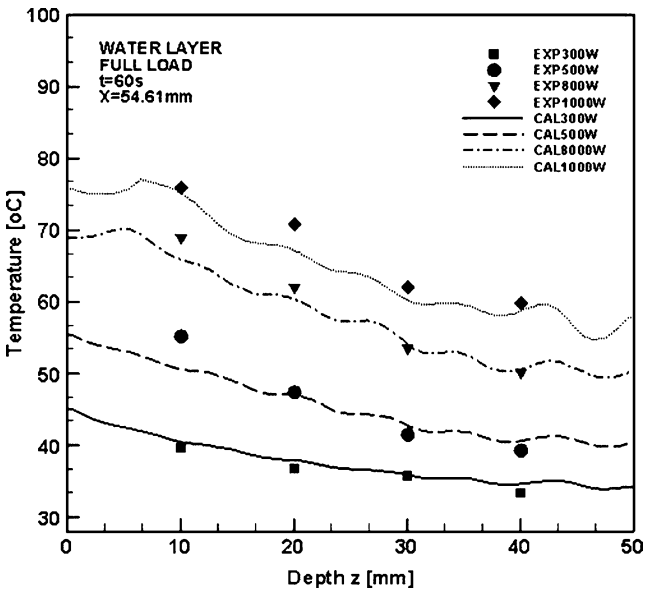

Fig. 6 Comparison of the temperature distribution within the water layer between the predicted and experimental results at various microwave power, at t=60 s, along with the vertical axis (x= 54.61 mm) of a rectangular wave guide

The Effect of Microwave Power

Figures 5 and 6 show the comparison of the temperature distribution within the water layer between the predicted and experimental results at various microwave power, at t= 60 s, along with the horizontal axis (z=10 mm) and vertical axis (x=54.61 mm) of a rectangular wave guide, respectively. Dimensions of water layer are 109.2(X)×54.61(Y) mm^2, which is equal to the size of wave guide. Thickness (Z) is 50 mm. It is found that power significantly influences the rate of temperature rise. Greater power provides greater heat generation rate inside the medium, thereby increasing the rate of temperature rise. Figure 5 shows the greatest temperature in the center of heating layer with the temperature decreasing toward the side walls of the water layer corresponding to the characteristic of TE_{10} mode. However, the results from calculation at the side walls are increasing, which is due to the walls being insulated and low rate of heat loss. In Fig. 6, the temperature within the water layer closest to the incoming microwave is shown. The region close to the top surface heats up with a faster rate than elsewhere within the water layer. Nevertheless, the temperature decays slowly along the propagation direction due to the skin depth heating effect. The predicted results are in a reasonable agreement with the experimental results.

Figure 7a and b shows simulation of electric field. Figure 7a is the case of empty wave guide. Figure 7b is the

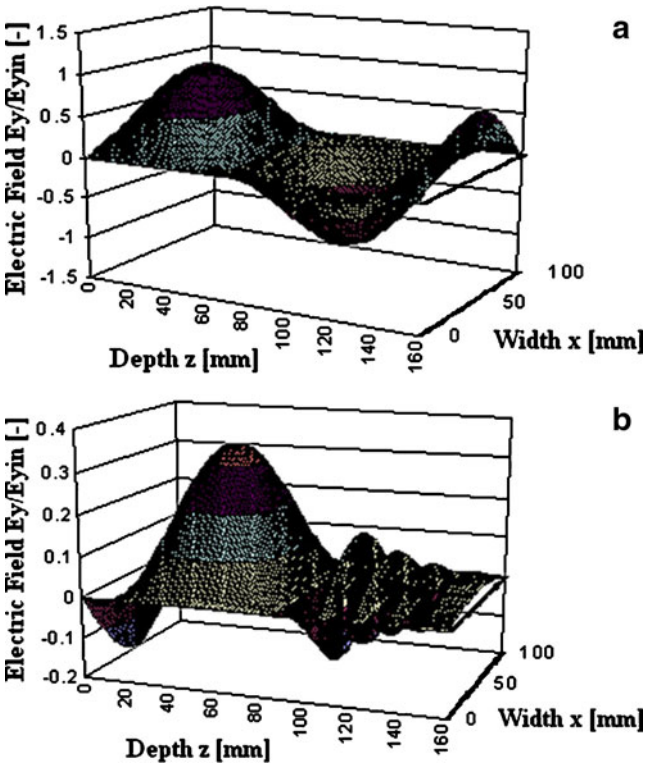

Fig. 7 Distribution of electric field (P=300 W): **a** wave guide is empty, **b** insert water layer

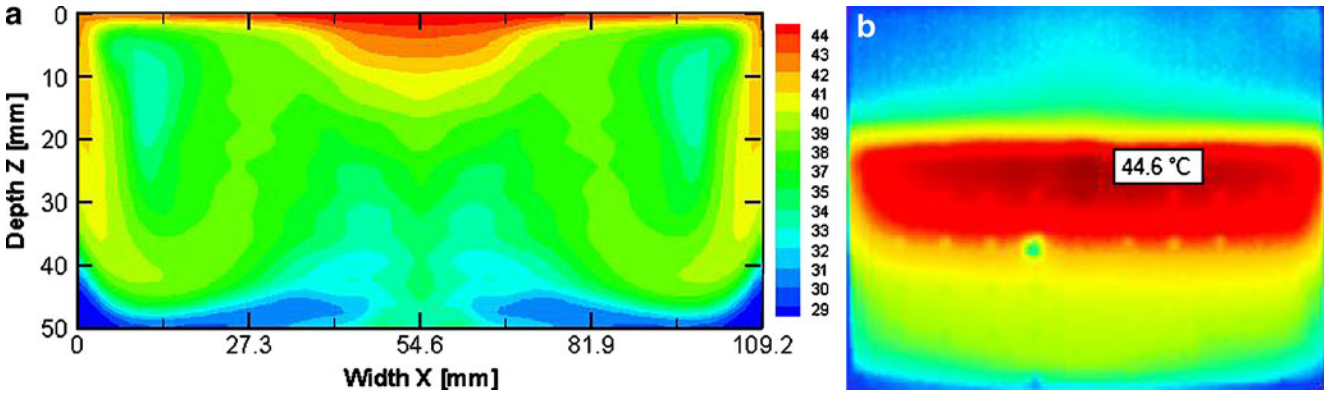

Fig. 8 Temperature profiles within water layer on *X–Z* plane (*P*=300 W, *t*=60 s): **a** from calculation, **b** captured by infrared camera

case of water layer inside wave guide. The vertical axis represents the intensity of the electric field E_y, which is normalized to the amplitude of the input electromagnetic wave E_{yin}. Figure 7a is the simulated electric field of TE_{10} mode along the center axis x=54.61 mm of a rectangular wave guide. For this case, the inside of the wave guide is empty, and the incident wave is chosen to be 9.565×10^3 V/m (300 W). A uniform static wave of TE_{10} mode inside wave guide is shown. Figure 7b shows a stronger standing wave with a larger amplitude forms in the cavity forward to the water layer, while the electric field within the water layer is extinguished. Since the incident wave passing through the cavity having low permittivity is directly irradiated with the water layer having high permittivity, the major part of incident wave is reflected and resonated, while other part that is minor is transmitted.

Figure 8a and b shows temperature profiles from calculation and that captured by infrared camera, respectively. Microwave power is 300 W (*t*=60 s). The results agree reasonably well.

Figures 9a and b shows temperature profiles within a water layer on *X–Z* plane at various microwave power (300 and 1,000 W). In the case of a full load, a temperature profile is symmetric. The left figure shows early state (*t*=20 s), and the right figure shows final state (*t*=60 s). The highest temperature in the upper region of heating water

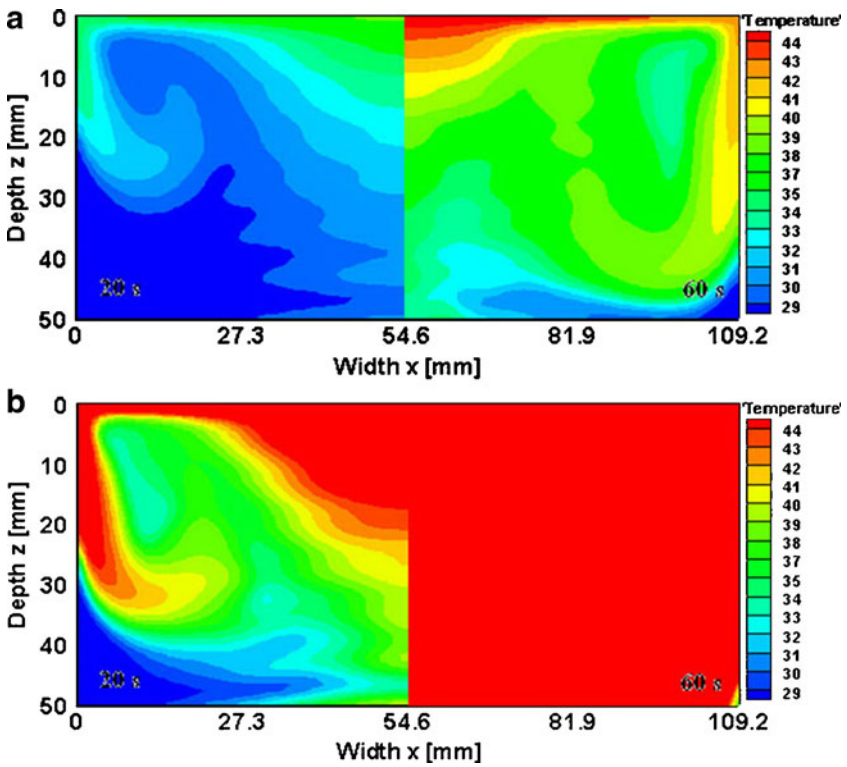

Fig. 9 Temperature profiles within water layer on *X–Z* plane at various microwave power: **a** 300 W, **b** 1,000 W

layer with the temperature decreasing towards the lower wall is shown.

Figures 10a and c are velocity fields within water layer on X–Z plane, corresponding to temperature fields in Fig. 9a and b. At the early stage of heating (t=20 s), the effect of conduction plays the greatest role than convection mode. As the heating proceeds, the local heating on the surface water layer causes the difference of surface tension on the surface of water layer, which leads to the convective flow of water (Marangoni flow). This causes water to flow from the hot region (higher power absorbed) at the central region of water layer to the colder region (lower power absorbed) at the side wall of container. In the stage of heating (t=60 s), the effect of convective flow becomes stronger and plays a more important role, especially at the upper portion of the side walls of container. However, at the bottom region of the walls where the convection plays the smallest, temperature distributions are primarily governed by the conduction mode. In the case of microwave power level of 300 W, the temperature within water layer is greater closer to the incoming microwave and has a trend corresponding to those of velocity fields.

In the case of microwave power level of 1,000 W, overall, temperature is greater near the top surface and locally high inside the layer. Furthermore, it is evident that the heating rate is higher in this case than in 300 W. This is because of the penetration depth heating effect, which increases a larger part of the incident wave to penetrate further into the water layer.

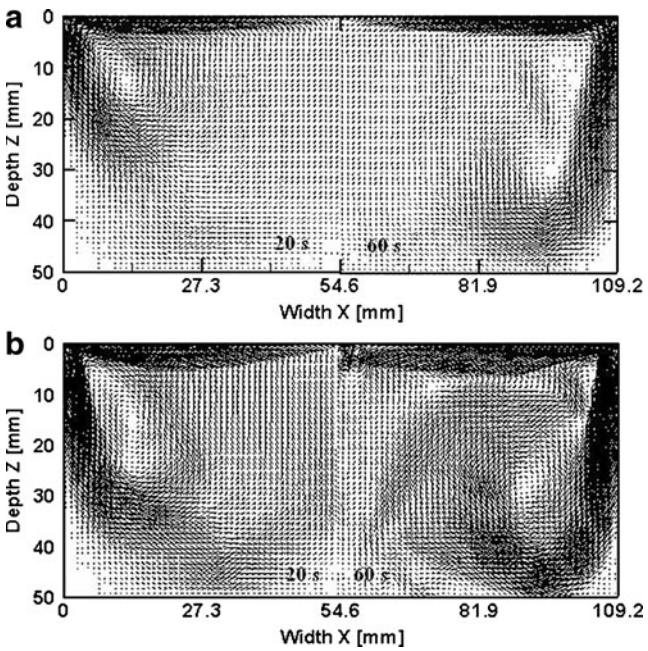

Fig. 10 Velocity field within water layer on X–Z plane at various microwave power: **a** 300 W and **b** 1,000 W

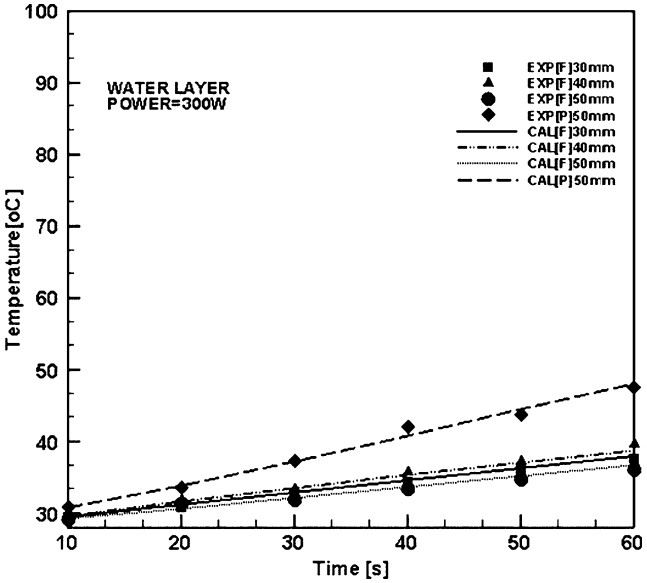

Fig. 11 The comparison of the temperature distribution within the water layer between the predicted and experimental results at various sample sizes

The Effect of Liquid Layer Size

Figure 11 shows the comparison of the temperature distribution within the water layer between the predicted and experimental results at various sample sizes. Microwave power is 300 W. From the figure, dimensions of water layer are $54.61(X)\times54.61(Y)\times50(Z)$ mm^3, providing the highest heat generation rate within sample. This is because water that has a smaller volume has a higher rate change of

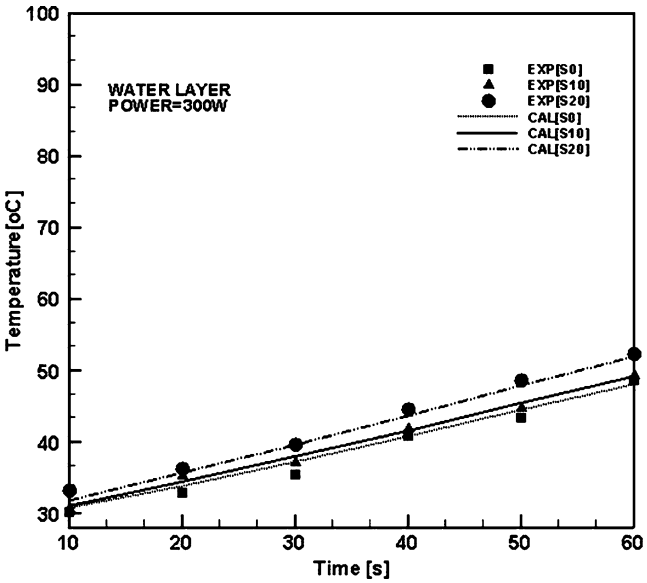

Fig. 12 The comparison of the temperature distribution within the water layer between the predicted and experimental results at various positions inside wave guide

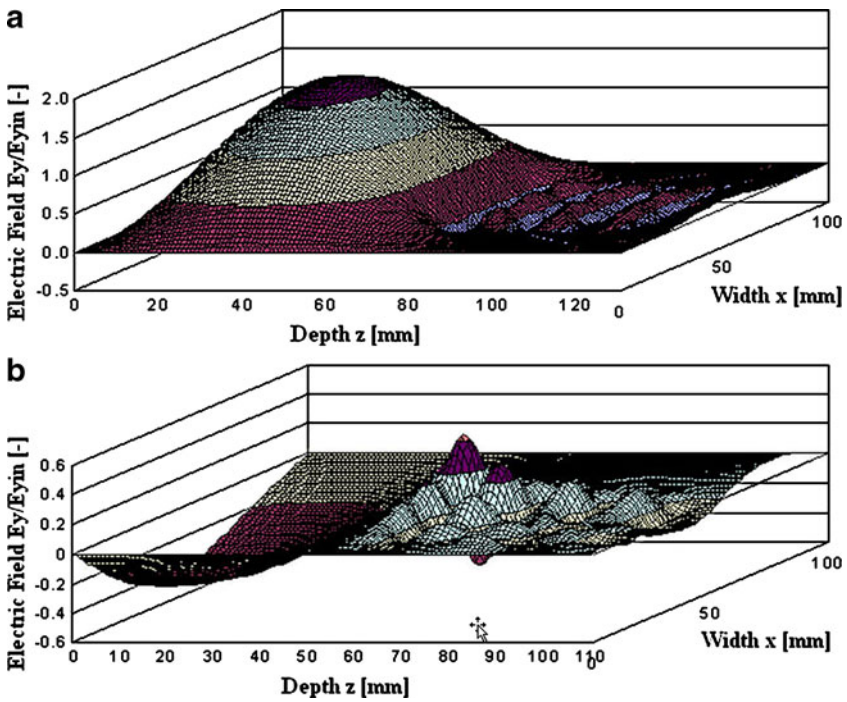

Fig. 13 Distribution of electric field at various positions inside wave guide: **a** S0, **b** S20

temperature due to larger heat generation rate per unit volume. However, the exception is observed. Although the water in a 109.2(X)×54.61(Y)×40(Z)-mm^3 container has larger volume than that in a 109.2(X)×54.61(Y)×30 (Z)-mm^3 container, the water with the larger volume has greater rate of temperature rise. The reason behind this result is that the penetration depth of water that is greater than its thickness causes the interference of waves reflected

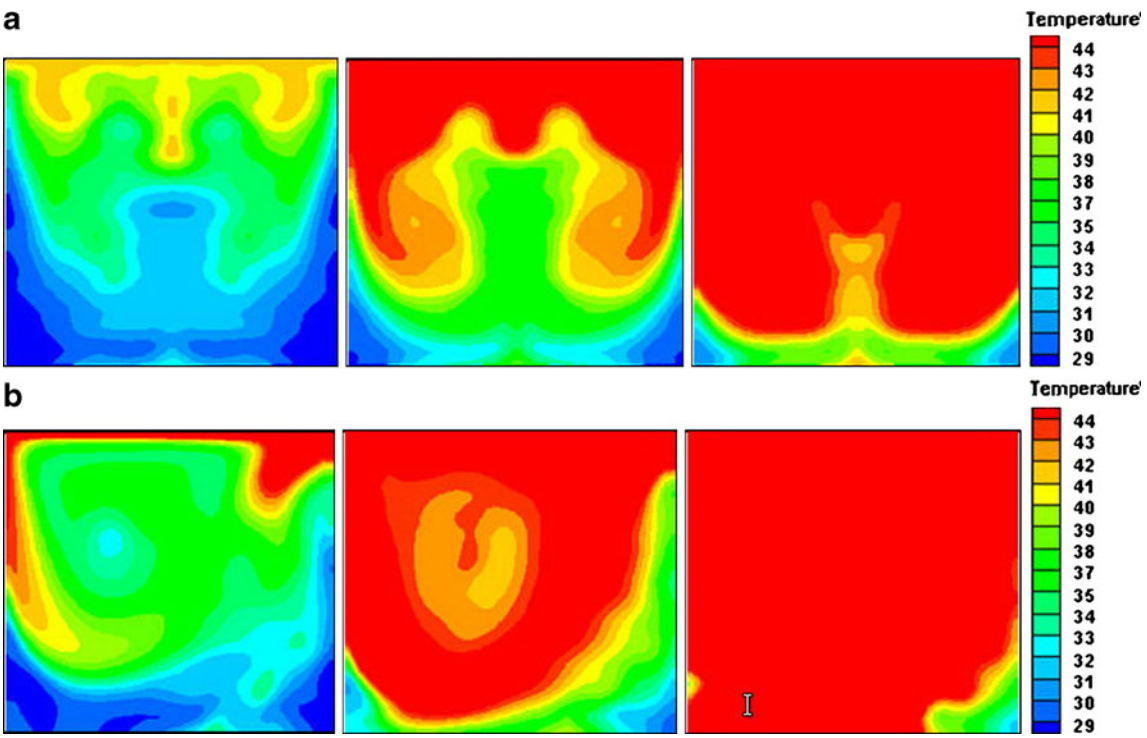

Fig. 14 Temperature profiles within water layer in case of partial load at various positions inside wave guide (P=300 W, thickness=50 mm): **a** S0, **b** S20

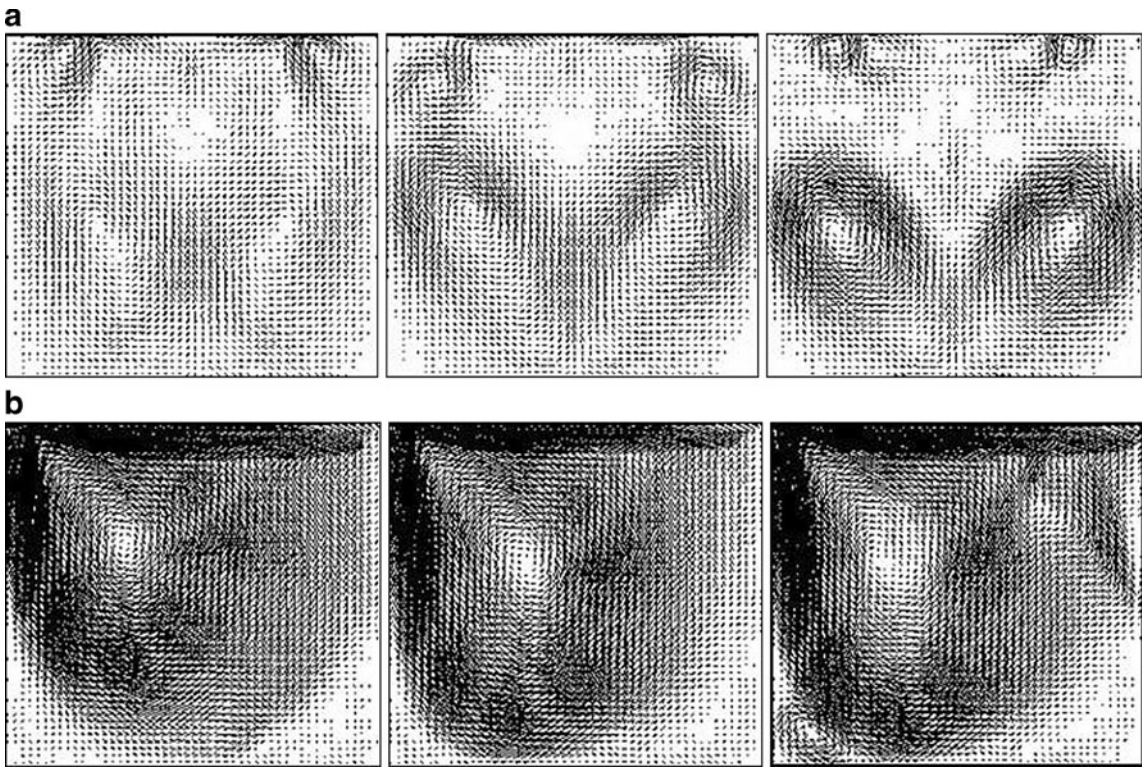

Fig. 15 Velocity field within water layer in case of partial load at various positions inside wave guide (P=300 W, thickness=50 mm); **a** S0, **b** S20

from the interface of water and air at the lower side due to the difference of dielectric properties of water and air. Consequently, the reflection and transmission components at each interface contribute to the resonance of standing wave inside the water sample. Therefore, the field distribution does not poses an exponential decay from the surface.

The Effect of Position of Liquid Layer Inside Wave Guide

This section discusses the effects of positions of the water layer in the rectangular wave guide. Three different locations of the water layer are investigated. The dimension of the water layer is 54.61(X)×54.61(Y) mm^2 and is 50(Z) mm in thicknesses.

Figure 12 shows the comparison of the temperature distribution within the water layer between the predicted and experimental results at various positions inside wave guide. Microwave power is 300 W. From these figure, the rate change of temperature is highest when the location of the sample is shifted to 20 mm away from the center, whereas the rate is lowest when the sample is located at the center.

Figures 13, 14, and 15 show phenomena of microwave heating of water layer in case of partial load at various positions (P=300 W).

Figure 13a and b shows the distribution of electric field within water layer. It shows considerably uniform distribution of electric field when the sample is located at the center (S0), whereas distribution of electric field is relatively not uniform when location of the sample is shifted to 20 mm away from the center, which is denoted by S20.

Figure 14a and b presents temperature profiles within the water layer on X–Z plane. Figure 14a shows the distribution of temperature when the sample is located at the center (S0). Temperature profile is symmetrical and is similar in the case of full load. The upper region of heating is a high temperature and decreases towards the lower wall. However, the wall side has temperature greater than the center of

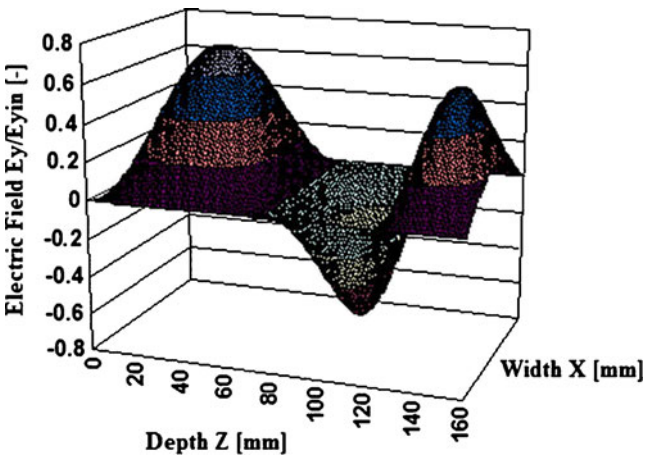

Fig. 16 Distribution of electric field inside wave guide and oil

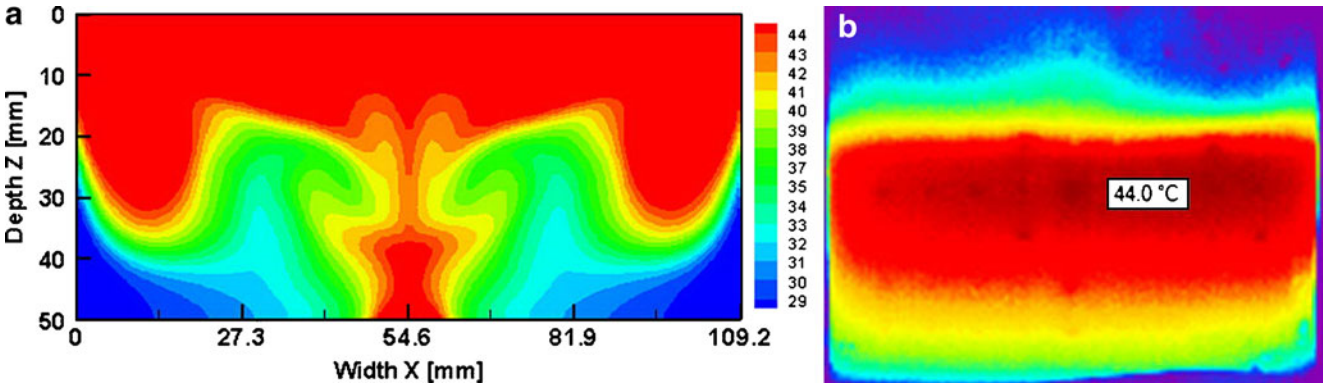

Fig. 17 Temperature profiles within oil on *X*–*Z* plane at 60 s; **a** from calculation, **b** captured by infrared camera

water layer. Figure 14b shows the distribution of temperature when location of the sample is shifted to 20 mm away from the center. Temperature profile is not symmetrical. The temperature distributes from the corner of the sample toward the lower side. In addition, it is interesting that the rate change of temperature becomes greatest when the sample is displaced 20 mm from the center. This result is attributed to the size of sample that is smaller than the wave guide; therefore, waves reflect disorder resulting in a multimode of field pattern.

Velocity fields within water layer on *X*–*Z* plane are shown in Fig. 15a and b. Several circulations are observed in Fig. 14a and b. When location of the sample is shifted to 20 mm away from the center, there appears the transition from several circulations to one larger circulation. The vectors are rigorous near the upper left corner. The velocity fields have a trend corresponding to that of temperature profiles.

The Effect of Dielectric Properties

Microwave-heating process within water layer and oil are examined in this section. The samples used are water and cooking oil. For the water layer, the physical phenomena of microwave heating are shown in the preceding sections. Temperature is highest at the center since the density of the electric field of the microwave field in the TE_{10} mode is high around the center region in the wave guide. The temperature is higher closer to the surface of water since water is a high lossy dielectric material, which has a small penetration depth causing the field to decay rapidly. The penetration depth is computed using Eq. 7 based on the dielectric properties of water.

Next, the result of oil can be observed in Fig. 16, 17, and 18, which respectively present the electric field distribution, contours of temperature, and velocity field. The dimension of oil layer is $109.2(X)\times54.61(Y)\times50(Z)$ mm^3. Figure 16 depicts the surface plots of simulation of electric field inside wave guide and oil along the center axis $x=$ 54.61 mm of a rectangular wave guide. Microwave power is 300 W (9.565×10^3 V/m). Figure 17a and b shows temperature profiles from the calculation and that captured by infrared camera, respectively. The results agree reasonably well. The temperature is highest in the upper region of the heating oil, with the temperature decreasing towards the lower wall. This oil is considered a low lossy material in which the fields can penetrate farther than in the water layer, causing high temperature at the lower region of the layer. Furthermore, the temperature distribution of oil (Fig. 17) and water (Fig. 8) are compared. It is found that temperature in the *X*–*Z* plane is more uniform in water than in oil, since more convection mechanism exists in water. The convection mode of heat transfer helps in distributing temperature throughout the layer. Figure 18 depicts flow pattern within the oil layer. The flow motions are induced by temperature gradients. The flow directions are indicated by the overwritten arrows significantly controlling overall heat transfer directions.

Conclusion

The numerical analysis in this paper describes many of the important interactions within a water layer and oil during

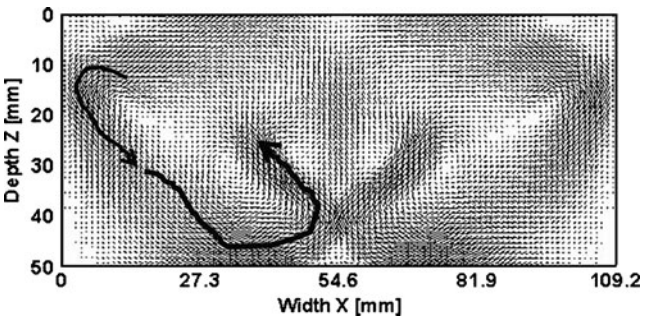

Fig. 18 Velocity field within oil layer in case of full load at 60 s ($P=$ 300 W, thickness=50 mm)

microwave heating using a rectangular wave guide. The following summarizes the conclusions of this work:

1. A mathematical model of microwave heating by using rectangular wave guide is presented, which is in relatively good agreement with the results of the experiment. The model used successfully describes the heating phenomena of water layers and oil under various conditions.
2. The temperature profiles and velocity fields in the water layer and oil are governed by the electric field as well as dielectric properties of water.
3. The distribution of heating location primarily depends on the penetration depth of liquid layer.
4. Size and thickness of water layer have an effect on phenomena of microwave heating. Water layer that is small and has thickness close to penetration depth has greater distribution of temperature due to larger heat generation rate per unit volume, and the reflection and transmission components at each interface contribute to a stronger resonance of standing wave inside the sample.
5. The position of water layer inside the wave guide is proven to have an important effect on microwave heating process. When the layer is placed off the center, it reveals unsymmetrical heating and flow patterns, which enhance the rate of temperature rise.
6. Natural convection due to buoyancy force strongly affects flow pattern within water layer during microwave heating process and clearly enhances temperature distribution in the layer.

The next steps of this research will be to investigate more associated parameters and more details of position inside wave guide and develop the 3D mathematical model.

Acknowledgement The authors gratefully acknowledge the financial support provided by The Thailand Research Fund for the simulation facilities described in this paper.

References

Aparna, K., Basak, T., & Balakrishnan, A. R. (2007). Role of metallic and composite (ceramic–metallic) supports on microwave heating porous dielectrics. *International Journal of Heat and Mass Transfer*, *50*, 3072–3089. doi:10.1016/j.ijheatmasstransfer.2006.11.021.

Ayappa, K. G., Brandon, S., et al. (1994). Microwave driven convection in a square cavity. *AIChE Journal*, *40*(7), 1268–1272. doi:10.1002/aic.690400718.

Basak, T. (2003). Analysis of resonance during microwave thawing of slabs. *International Journal of Heat and Mass Transfer*, *46*, 4279–4301. doi:10.1016/S0017-9310(03)00212-6.

Basak, T. (2004). Role of resonance on microwave heating of oil–water emusions. *AIChE Journal*, *50*, 2659–2675. doi:10.1002/aic.10207.

Basak, T., & Ayappa, K. G. (2002). Role of length scales on microwave thawing dynamics in 2D cylinders. *International Journal of Heat and Mass Transfer*, *45*(23), 4543–4559. doi:10.1016/S0017-9310(02)00171-0.

Boyacı, İ. H., Sumnu, G., & Sakiyan, O. (2009). Estimation of dielectric properties of cakes based on porosity, moisture content, and formulations using statistical methods and artificial neural networks. *Food Bioprocess Technology*. doi:10.1007/s11947-008-0064-z

Chatterjee, S., Basak, T., & Das, S. K. (2007). Microwave driven convection in a rotating cylindrical cavity, A numerical study. *Journal of Food Engineering*, *79*, 1269–1279. doi:10.1016/j.jfoodeng.2006.04.039.

Curet, S., Rouaud, O., & Boillereaux, L. Microwave tempering and heating in a single-mode cavity: Numerical and experimental investigations. *Chemical Engineering and Processing*, *47*, 1656–1665.

Datta, A. K., Prosetya, H., & Hu, W. (1992). Mathematical modeling of batch heating of liquids in a microwave cavity. *Journal of Microwave Power and Electromagnetic Energy*, *27*, 38–48.

Dibben, D. C., & Metaxas, A. C. (1997). Frequency domain vs. time domain finite element methods for calculation of fields in multimode cavities. *IEEE Transactions on Magnetics*, *33*(2), 1468–1471. doi:10.1109/20.582537.

Huo, Y., Li, B. Q., & Tang, J. (2004). Boundary/finite edge element modeling of 3-D microwave thermal food processing. ASME, Heat Transfer Division, (Publication) HTD 375 (1), Art. No. IMECE2004-59670, pp. 687–694.

Jia, X., & Bialkowski, M. (1992). Simulation of microwave field and power distribution in a cavity by a three dimension finite element method. *Journal of Microwave Power and Electromagnetic Energy*, *27*(1), 11–22.

Liu, F., Turner, I., & Bialowski, M. (1994). A finite-difference time-domain simulation of power density distribution in a dielectric loaded microwave cavity. *Journal of Microwave Power and Electromagnetic Energy*, *29*(3), 138–147.

Mur, G. (1981). Absorbing boundary conditions for the finite-difference approximation of the time-domain electromagnetic-field equations. *IEEE Transactions on Electromagnetic Compatibility EMC-23*, *4*, 377–382. doi:10.1109/TEMC.1981.303970.

Patankar, S. V. (1980). *Numerical heat transfer and fluid flow*. New York: Henisphere.

Ratanadecho, P., Aoki, K., & Akahori, M. (2002a). A numerical and experimental investigation of the modeling of microwave heating for liquid layers using a rectangular wave guide (effects of natural convection and dielectric properties). *Applied Mathematical Modelling*, *26*, 449–472. doi:10.1016/S0307-904X(01)00046-4.

Ratanadecho, P., Aoki, K., & Akahori, M. (2002b). Experimental validation of a combined electromanetic and thermal model for a microwave heating of multi-layered materials using a rectangular wave guide. *ASME Journal of Heat and Transfer*, *124*(5), 992–996. doi:10.1115/1.1495521.

Rattanadecho, P. (2006). The simulation of microwave heating of wood using a rectangular wave guide: Influence of frequency and sample size. *Chemical Engineering Science*, *61*, 4798–4811. doi:10.1016/j.ces.2006.03.001.

Rattanadecho, P., Kazuo, A., & Masatoshi, A. (2002). The characteristics of microwave melting of frozen packed beds using a rectangular wave guide. *IEEE Transactions on Microwave Theory and Technique*, *50*(6), 1487–1494. doi:10.1109/TMTT.2002.1006410.

Rattanadecho, P., & Suwannapum, N. (2009). Interactions between electromagnetic and thermal fields in microwave heating of hardened type I-cement paste using a rectangular wave guide (influence of frequency and sample size). *ASME Journal of Heat and Transfer* (in press).

Tada, S., Echigo, R., & Yoshida, H. (1997). Numerical analysis of electromagnetic wave in a partially loaded microwave applicator.

International Journal of Heat and Mass Transfer, *41*, 709–718. doi:10.1016/S0017-9310(97)00164-6.

Vadivambal, R., & Jayas, D. S. (2009). Non-uniform temperature distribution during microwave heating of food materials—A review. *Food Bioprocess Technology.* doi:10.1007/s11947-008-0136-0

Yee, K. S. (1996). Numerical solution of initial boundary value problems involving Maxwell's equation in isotropic media. *IEEE Transactions on Antennas and Propagation*, *14*, 302–307.

Zhang, Q., Jackson, T. H., & Ungan, A. (2000). Numerical modeling of microwave induced natural convection. *International Journal of Heat and Mass Transfer*, *43*, 2141–2154. doi:10.1016/S0017-9310(99)00281-1.

Zhu, J., Kuznetsov, A. V., & Sandeep, K. P. (2007). Mathematical modeling of continuous flow microwave heating of liquid (effect of dielectric properties and design parameters). *International Journal of Thermal Sciences*, *46*, 328–341. doi:10.1016/j.ijthermalsci.2006.06.005.